PCCP

PAPER

View Article Online
View Journal

Cite this: DOI: 10.1039/c9cp01615e

Understanding chemical interaction between phosphonate-derivative molecules and a silver surface cluster in SERS: a combined experimental and computational approach†

Gauthier Emonds-Alt,‡[ab] Benoit Mignolet,‡[c] Cedric Malherbe,[a] Jean-Christophe M. Monbaliu,[b] Francoise Remacle[c] and Gauthier Eppe*[a]

The interaction between phosphonate functions and a silver surface cluster is investigated using Surface-Enhanced Raman Spectroscopy (SERS). Changing the functional group (methylphosphonic acid based molecule) by studying the effect of protonation, methylation and substitution of the side chain with amine and carboxylate functions enabled us to modulate the chemical interactions between the different functions and the metal cluster. We find that the adsorption energy of the methylphosphonic acid decreases with the protonation, the methylation processes and the substitution of the side chain. In all cases, only the deprotonated phosphonate forms are SERS active. To understand how the molecules interact with the nanoparticle, the electronic structure, adsorption energies and Raman spectra were computed for molecules adsorbed on a 20 atom silver cluster representing a nanoparticle surface. The qualitative agreement between computed static Raman spectra and experimental SERS spectra makes it possible to determine stable geometries of the analyte–silver cluster complexes and to characterize the adsorption modes. The findings presented here provide a framework for designing analytical developments based on SERS for simultaneous detection of phosphonated molecules, including pesticides such as glyphosate, creating practical opportunities in key areas such as environmental and water resource *in situ* monitoring.

Received 22nd March 2019,
Accepted 19th August 2019

DOI: 10.1039/c9cp01615e

rsc.li/pccp

Introduction

Phosphonates, *i.e.* alkyl or aryl esters of phosphonic acids, are organophosphorous compounds that have found various applications as pesticides, active pharmaceutical compounds and chelatants.[1] As such, they help to stabilize and functionalize nanoparticles. Liong M. *et al.* developed nanoprobes based on iron nanoparticles stabilized with phosphonate molecules (acting as stabilizing agent) for drug delivery.[2] In 2015, Li R. *et al.* developed nanoparticle probes for imaging, where phosphonate prevented the interferences of cellular phosphate.[3] Understanding the orientation, the structure and the bonding of small phosphonate-bearing molecules at the surface of a nanoparticle may therefore help to control the stability of phosphonate-nanoparticle based systems.

Adsorption processes of small molecules on the surface of metallic nanostructures are important for various applications. Functionalized nanoparticles are used in medicine,[3] biology,[4] analytical chemistry[5] and environmental chemistry.[6] The adsorption of small molecules on a metallic surface is affected by the chemical environment and is therefore often studied under restricted experimental conditions. However, the adsorption mechanisms are often neglected in applied research.

The adsorption of molecules on silver and gold surfaces can be investigated using experimental techniques such as Atomic Force Microscopy (AFM),[7] Scanning Tunneling Microscopy (STM),[8] Infrared (IR)[9] and X-Ray photoelectron spectroscopy (XPS).[10] Besides, Surface Enhanced Raman spectroscopy (SERS) is particularly sensitive to the molecular structure in the close vicinity of the nanoparticle.[11] SERS is based on the enhancement of the Raman scattering, which gives structural information of the target molecule. Usually, a Raman signal enhancement of the order of 10^4 to 10^6 is observed but the enhancement factor can reach 10^{14}–10^{15} allowing a single molecule to be detected.[12]

[a] *Mass Spectrometry Laboratory, MolSys Research Unit, University of Liège, B4000 Liège, Belgium. E-mail: g.eppe@uliege.be*
[b] *Center for Integrated Technology and Organic Synthesis, MolSys Research Unit, University of Liège, B4000 Liège, Belgium*
[c] *Theoretical Physical Chemistry, MolSys Research Unit, University of Liège, 4000 Liege, Belgium*

† Electronic supplementary information (ESI) available: Explicit solvation, isomers of the analyte–silver cluster complexes and full Raman spectra between 0 and 2000 cm^{-1}. See DOI: 10.1039/c9cp01615e

‡ G. Emonds-Alt and B. Mignolet contributed equally to this work.

The SERS effect can be explained by two enhancement mechanisms: (i) the electromagnetic enhancement and (ii) the chemical enhancement. The electromagnetic mechanism explains the enhancement of the local electromagnetic field near the metallic surface resulting from the excitation of the surface plasmon of the nanoparticles. The magnitude of the electric field $|E|$ is much higher near the nanoparticles than far away from their surface. The electric field decreases with the distance to the nanoparticle surface following a d^{-3} relationship. The SERS signal, which is proportional to $|E|^4$, decreases therefore in d^{-12}. On the other hand, the chemical enhancement, much weaker than the electromagnetic mechanism, is due to the interaction between the metallic nanoparticle and the target molecule forming a complex. Therefore, SERS spectroscopy is an effective technique for investigating interfacial properties. Studying the frequency shifts and the relative intensities of SERS bands provides information on the average conformation and relative proximity of different chemical functions of the adsorbed molecule at the metallic surface. Electronic structure computations provide additional information on the enhanced vibrational modes and on the adsorption site of the molecule on the surface. Few research studies on the investigation of the adsorption of phosphonate derivatives on a silver surface have been carried out using SERS. Podstawka E. *et al.* studied the interaction of phosphonate derivatives of imidazole, thiazole and pyridine at the surface of a silver electrode in order to demonstrate the feasability of using SERS spectroscopy to probe interactions that mimic the mechanism of a substrate binding to its receptor.[13] Costa J. C. S. *et al.* correlated experiments with a theoretical study. They computed the electronic structure of organophosphorus pesticides (such as (*N*-phosphonomethyl)glycine commonly known as glyphosate) in close contact with a single silver atom. Finally, they compared SERS spectra of these molecules with computed compounds in order to demonstrate how molecules interact with the silver surface.[5] Proniewicz L. M. *at al.* have also studied the adsorption geometry of *N*-benzylamino(boronphenyl)-methylphosphonic acids and boron derivatives of aminophosphonic acids on silver surfaces by combining theoretical methods with experimental SERS measurements.[14,15]

The main objective of this study is to understand the interaction between the phosphonate function and a silver surface using SERS. Methylphosphonic acid, and four of its derivatives have been studied to highlight (i) the effect of the protonation, (ii) the effect of the methylation of the phosphonate function and (iii) the effect of the substitution of the side chain in order to evaluate the affinity of the phosphonate function compared to an amine or a carboxylate function. To determine the adsorption site of these targeted molecules, adsorption energies and Raman spectra were computed for all molecules adsorbed on a 20 atom silver cluster that represents the NP surface. The good agreement between computed static Raman spectra and experimental SERS spectra provides insight into the adsorption mode of the phosphonate derivative molecules on silver nanoparticles.

Experimental

Materials

All the reagents were obtained from commercial sources and used without additional purification, except methyl hydrogen methylphosphonate, which was prepared by desmethylation of commercial dimethyl methylphosphonate. All solutions were prepared with water distillated twice.

Synthesis of silver nanoparticles

Silver nanoparticles (Ag NPs) were prepared by adapting the synthesis of Creighton[16] where silver cations are reduced with $NaBH_4$ according to eqn (1).

$$Ag^+ + BH_4^- \rightarrow Ag + \frac{1}{2}H_2 + \frac{1}{2}B_2H_6 \quad (1)$$

Typically, an aqueous solution of $AgNO_3$ (2.5 mM, 50 mL, cooled at 1 °C) was added dropwise to a vigorously stirred aqueous solution of $NaBH_4$ (2 mM, 150 mL) maintained at 1 °C in an ice bath. Diborane subsequently reacts with water to form boric acid that is adsorbed at the surface of the Ag NPs, thereby stabilising them.

$$B_2H_6 + 6H_2O \rightarrow 2H_3BO_3 + 6H_2 \quad (2)$$

The colloidal suspension was then heated at 90 °C for 45 minutes to eliminate the excess sodium borohydride. The residual solution was then adjusted to 200 mL and stored at 4 °C. The final solution displayed a yellow color. Spherical Ag NPs were obtained with an average diameter of 25 nm (as determined by Transmission Electron Microscopy) and are characterized with a maximum of visible light absorption at 393 nm (as determined by UV-Visible spectroscopy). The pH of the stored NP solution is 7.6.

Synthesis of the methyl hydrogen methylphosphonate

Methyl hydrogen methylphosphonate lithium salt was prepared adapting the protocol of H. Krawczyk.[17] A solution of dimethyl methyl phosphonate (20 mmol) and LiBr (20 mmol) in isobutyl methyl ketone (30 mL) was heated at 80 °C. After the appearance of a white precipitate, the reaction mixture was kept at 80 °C for 30 minutes. The solvent was then removed under reduced pressure. The hemisolid residue was taken up with diethyl ether (40 mL) and filtrated. The residue was washed with diethyl ether (20 mL), and dried for 1 h under vacuum. The purity of the methyl hydrogen methylphosphonate lithium salt was confirmed by ^{31}P and ^{1}H NMR in D_2O.

SERS measurements

All samples were prepared by adding 50 μL of aqueous solution of 1 mM of the target molecules (methylphosphonic acid, methyl hydrogen methylphosphonate, dimethyl methyl phosphonate, aminomethylphosphonic acid or glyphosate) to 500 μL of Ag NP suspension. The target molecules and Ag NPs were incubated for 30 min, then 50 μL of sodium ascorbate buffer (0.5 M) and 200 μL of aggregating agent ($NaNO_3$, 3.75 M) were successively added into disposable polystyrene cuvettes

prior to SERS measurements. The use of an aggregating agent is usually necessary for SERS measurements.[18,19] The pH of the solution was determined using a HAMILTON double pore pH electrode.

All SERS spectra were recorded with a Raman spectrometer Labram 300 from Horiba interfaced with an Olympus BX-40 confocal microscope and equipped with a 632.8 nm HeNe excitation laser. Raman spectra of the samples were obtained directly in polystyrene cuvettes using a 90° angled return mirror through an achromatic lens (focal distance of 50 mm) and a laser power of 4 mW at the sample. Every spectrum was accumulated twice for 10 s in the 650–1410 cm^{-1} range of Raman shift.

Computation details

All the computations on the bare Ag_{20} cluster (as a model to represent the nanoparticle surface) and on the target molecules adsorbed on the Ag_{20} cluster were carried out at the density functional theory (DFT) level with the polarizable continuum model (PCM) as implemented in Gaussian 09.[20] We used the long-range corrected functional wB97XD[21] that includes empirical dispersion (Grimme's D2 dispersion model), which is important to account for the weak and long-range interactions between the molecule and the Ag cluster. The basis sets are the LanL2DZ with Effective Core Potentials[22] for Ag atoms and the cc-pVDZ basis set for the adsorbed molecules. The vibrational frequencies at the equilibrium geometries of the stable complexes reported below and in the ESI† were all real. They were used to compute the Raman spectra that were isotropically averaged over the orientations. The largest component of the polarizability is that perpendicular to the surface of the cluster. The initial geometry of the bare Ag_{20} cluster was taken from Moore J. E. *et al.*,[23] where this cluster was used to compute the chemical enhancement of pyridine in SERS. The Ag_{20} cluster is neutral and closed shell. All the complexes investigated below are closed shell and computed in the singlet spin state.

The SERS experiments are carried out in water. To determine the equilibrium geometries and Raman spectra of a large number of the isomers of the Ag_{20}–analyte complexes, we used the PCM model and only discuss the effect of explicit solvation by H_2O molecules in the case of the $MePO_3^{2-}$ analyte. The PCM solvation model describes the polarization of the silver–analyte complex by the solvent. As discussed in the ESI,† neglecting explicit solvation might lead to a red shift of the P–C vibrational band and could affect the relative intensity of the symmetric and antisymmetric P–O stretching bands. Using explicit solvation by water molecules may lead to hydrogen bonds between the polar groups of the analyte (phosphonate or amine functions) and the hydrogen atoms of the water molecules. These interactions can also affect other bonds that are close to the polar groups. For the $MePO_3^{2-}$ anion, we find that adding explicit solvation triggers a shortening of the P–C bond and a blue shift of the P–C stretching frequency. Such blue shifts have been reported for 1,4-dioxane.[24]

Results and discussion

The SERS spectrum is representative of the molecular composition in proximity of the NP surface. Therefore, SERS spectroscopy is an interesting tool to study the adsorption mode of molecules on the surface of noble metal NPs (here silver NPs). The most intense Raman bands may be associated to chemical functions which are in the close vicinity of the NP surface.[25] However, nanoparticle surfaces are often coated by a stabilizing agent, either added after the synthesis or generated *in situ* during the synthesis, like here with H_3BO_3. Hence, the SERS spectrum of the subsequently added targeted molecules will only be observed if the targeted molecule has a larger affinity with the metallic surface than the stabilizing agent.

In order to determine whether a molecule will be SERS active or not, we computed the adsorption energies of the stabilizing agent and of the phosphonate-derivative molecules investigated in this study (see Table 1 and computational details). The adsorption energy of a given targeted molecule (TM) is computed as $E_{TM} = (E_{Ag_{20}} + E_{TM}) - E_{Ag_{20}\text{-}TM}$, where the nanoparticle is approximated by a 20-atom silver cluster. If the adsorption energy of the targeted molecule is larger than the adsorption energy of the stabilizing agent, then the targeted molecule could displace the stabilizing agent and lead to a SERS activity.

Table 1 Computed adsorption energies and selected Ag–O bond lengths of the different protonation forms of the phosphonate–Ag_{20} complexes as well as of the complexes with boric acid (DFT/wB97XD level see computational details). The adsorption energy E_a is defined as $E_a = (E_{Ag_{20}} + E_{analyte}) - E_{complex}$

Molecule	Adsorption energy (kcal mol^{-1})	Bond	Bond length (Å)
$(CH_3\text{–}PO_3)^{2-}$	51.5	AgO	2.29
			2.32
			2.33
$(CH_3\text{–}PO_3H)^{-}$	22.6	AgO	2.39
			2.42
		AgO–H	2.64
$(CH_3\text{–}PO_3H_2)^{0}$	13.6	AgO	2.40
		AgO–H	3.48
			3.60
$(CH_3\text{–}PO_2(OCH_3))^{-}$	28.5	AgO	2.33
			2.41
		Ag H_3C–O	3.25
$(CH_3\text{–}PO(OCH_3)_2)^{0}$	17.0	AgO	2.50
		Ag H_3C–O	2.86
			3.62
$(NH_2\text{–}CH_2\text{–}PO_3)^{2-}$ (θ_3)	49.3	AgO	2.29
			2.32
			2.33
$(NH_3\text{–}CH_2\text{–}PO_3)^{-}$ (θ_2)	21.6	AgO	2.38
			2.41
		AgO–H	3.21
$(OOC\text{–}CH_2\text{–}NH_2\text{–}CH_2\text{–}PO_3)^{2-}$ (θ_3)	37.7	AgO	2.31
			2.35
			2.40
$(OOC\text{–}CH_2\text{–}NH_2\text{–}CH_2\text{–}PO_3H)^{-}$ (θ_2)	19.2	AgO	2.37
			2.46
		AgO–H	2.73
H_3BO_3	8.6		
$(H_3BO_3)_2$	13.6		
$(H_3BO_3)_3$	21.9		

In this study, the affinity of 5 phosphonic derivatives (Fig. 1) with a silver NP's surface was evaluated and the corresponding adsorption modes on the silver cluster were determined by comparing the computed static Raman spectrum with the experimental SERS spectrum. In particular three molecular parameters were investigated:

(a) The effect of the protonation state of the molecule. The native methylphosphonic acid bears 2 acidic positions in the direct vicinity of phosphorus.

(b) The effect of methylation.

(c) The effect of side chain substitution.

To determine the lowest energy conformer of each of the 5 phosphonic derivatives investigated for different protonation states, several isomers of the Ag_{20}–analyte complexes exhibiting different binding sites or rotational angles were investigated. We report on the most stable isomer in the text and a selection of the other stable isomers and conformers are given in the ESI.† The qualitative agreement between the computed experimental SERS spectrum with the Raman spectrum of the Ag_{20}–analyte complex allows us to determine how the analyte will likely bind to the silver surface in the experiments.

(a) The effect of the protonation of the phosphonate.

Phosphonate is a functional group with three possible protonated forms, which can influence its adsorption on a NP's surface. We investigated the effect of the protonation of the phosphonate function by recording the SERS spectra of methylphosphonic acid (pK_{a_1} = 2.12 and pK_{a_2} = 7.29) at pH = 4 and pH = 9, where the phosphonate function is respectively singly deprotonated ($MePO_3H^-$) and doubly deprotonated ($MePO_3^{2-}$). In the SERS spectra shown in Fig. 2, the major difference occurs between 700 and 800 cm^{-1}. The totally deprotonated form (at pH = 9) has a single Raman band at 760 cm^{-1} while the singly deprotonated form (at pH = 4) has two Raman bands located at 730 cm^{-1} and 765 cm^{-1}. Between 800 and 1400 cm^{-1}, the Raman bands are located at identical Raman shifts, yet the relative intensities vary with the pH. These variations observed in experimental SERS spectra should be correlated to the presence or absence of protons on the phosphonate function.

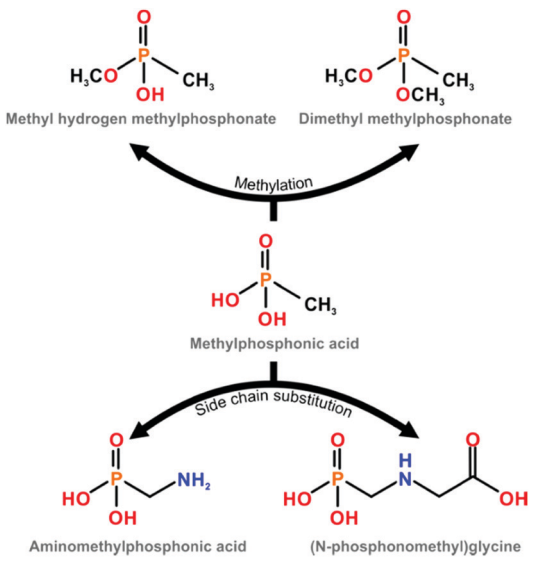

Fig. 1 Phosphonate derivatives investigated in SERS in this study.

To determine the adsorption site of $MePO_3H^-$ and of $MePO_3^{2-}$ on the NP, we computed the equilibrium geometry and frequencies of the lowest energy isomers of the $(Ag_{20}–MePO_3)^{2-}$ and $(Ag_{20}–MePO_3H)^-$ complexes and compared their computed Raman spectra to the experimental SERS spectra. The computed Raman spectra take explicitly into account the interaction of the molecule with the silver cluster and the interaction with the solvent *via* the PCM model. We compared the computed Raman spectra of $(Ag_{20}–MePO_3H)^-$ and of $(Ag_{20}–MePO_3)^{2-}$ to the SERS spectra of the methylphosphonic acid at pH = 4 and pH = 9 (Fig. 2F and B), respectively. The spectra exhibit three main regions (see Fig. 2) corresponding to the P–C, P–O and methyl normal modes.

As in the experimental spectrum, the computed spectra of the two deprotonated forms exhibit 1 and 2 Raman bands in the region between 700 and 800 cm^{-1} respectively. The doubly deprotonated form (pH = 9) only has one Raman band at 725 cm^{-1} (Fig. 2C and D) which corresponds to a delocalized normal mode composed mainly of the symmetric stretching of the P–C. The singly deprotonated form (pH = 4) has two Raman bands at 708 cm^{-1} and 763 cm^{-1} corresponding respectively to the symmetric (HO)–P–C stretching normal mode and to the anti-symmetric (HO)–P–C one (Fig. 2F). Therefore, the number of bands between 700 and 800 cm^{-1} is clearly indicative of the protonation form of the phosphonate function. In the two protonated forms of methylphosphonate, the P–C Raman band is red shifted compared to the experimental one because the hydrogen bonding between the oxygen of the phosphonate and the water molecules is not accounted for at the PCM level (see ESI,† see Fig. 2D). Adding three water molecules close to the phosphonate functional group for the $(Ag_{20}–MePO_3)^{2-}$ complex induces a blue shift of the P–C band (Fig. 2C). In addition, the Raman band computed for explicit solvation by H_2O molecules is broader with a shoulder peak similar to the experimental one. Adding 25 H_2O molecules around the isolated $MePO_3^{2-}$ (without the Ag_{20} cluster) anion provides a complete solvation shell and enhances the blue shift compared to explicit solvation with 3 H_2O molecules, which is in agreement with the experimental spectrum for the position of the band (Fig. S1, ESI†). We therefore expect that using a complete solvation shell around the $(Ag_{20}–MePO_3)^{2-}$ would lead to a good agreement with the experimental spectrum.

The computed Raman bands between 900 and 1200 cm^{-1} correspond to the symmetric and antisymmetric P–O stretching. These vibrational modes are strongly influenced by the silver atoms of the cluster nearby as well as by the solvent. Due to the small size of the Ag_{20} cluster, there is only one binding pattern: the phosphonate function is found to interact with three silver atoms that are at the edge of the Ag_{20} cluster. In the experimental spectra, we observed a broad pattern between 900 and 1200 cm^{-1}, with multiple peaks. Ligands typically bind close to the defects on the surface of the NP because those sites are more reactive.

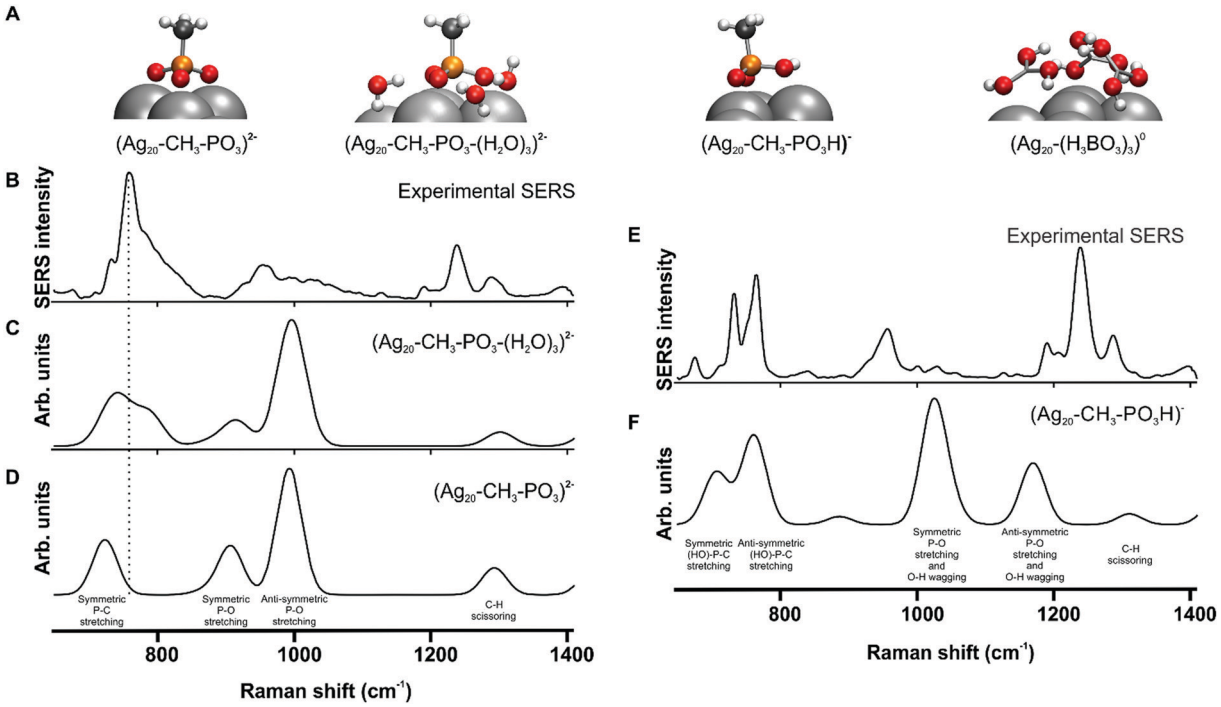

Fig. 2 (A) Equilibrium geometries of the adsorption mode of the analyte on the silver cluster for the $(Ag_{20}–CH_3PO_3)^{2-}$, $(Ag_{20}–CH_3PO_3–(H_2O)_3)^{2-}$ and $(Ag_{20}–CH_3PO_3H)^{-}$ complexes and for the trimer of stabilizing agent $(Ag_{20}–(H_3BO_3)_3)^{0}$. The color code is red for the oxygen atoms, white for the hydrogen atoms, grey for the carbon atoms, orange for the phosphorous atom and silver for the silver atoms (the van der Waals radii is shown). (B) Experimental SERS spectrum of methylphosphonic acid at pH = 9 where the doubly-deprotonated form ($CH_3–PO_3^{2-}$) dominates. (C) Lowest energy isomer of the $(Ag_{20}–MePO_3)^{2-}$ complex that has been explicitly solvated by 3 water molecules. (D) Computed Raman spectrum of lowest energy isomer of the $(Ag_{20}–MePO_3)^{2-}$ complex. (E) Experimental SERS spectrum of methylphosphonic acid at pH = 4 where the singly-deprotonated form ($CH_3–PO_3H^{-}$) dominates. (F) Computed Raman spectrum of lowest energy isomer of the $(Ag_{20}–MePO_3H)^{-}$ complex.

The broad peak reflects the variety of binding sites available on the NP surface while there is only one available for the Ag_{20} cluster. In addition, the solvent can interact with the molecule and change the relative intensity of the symmetric and antisymmetric P–O stretching bands as reported in the ESI† (Fig. S1).

The band corresponding to the methyl breathing is localized at 1310 cm^{-1} in $(Ag_{20}–MePO_3H)^{-}$ and $(Ag_{20}–MePO_3)^{2-}$, which is blue shifted by about 50 cm^{-1} compared to the experimental band. The computed spectra do not reproduce the fine structure that may arise from the relative orientation of the methyl with respect to the phosphonate function (staggered or eclipse conformation, see ESI†). At the equilibrium geometry of $(Ag_{20}–MePO_3H)^{-}$ and $(Ag_{20}–MePO_3)^{2-}$ complexes, the methyl is staggered with respect to the phosphonate function but the eclipse conformation is only 2.5 kcal mol^{-1} less stable so both conformers might be present in solution.

The qualitative agreement between the computed Raman spectra and the experimental SERS spectra suggests that the target molecules are adsorbed on the NP at pH = 9 and pH = 4 as in the lowest energy isomer of $(Ag_{20}–MePO_3H)^{-}$ and $(Ag_{20}–MePO)_3{}^{2-}$. In the complex $(Ag_{20}–MePO_3)^{2-}$, the three oxygen atoms of the totally deprotonated molecule interact with three silver atoms of the cluster in a top configuration. The Ag–O bond lengths are between 2.29 and 2.33 Å (tridentate mode, Fig. 2A). The successive protonation of the phosphonate group leads to the bidentate and monodentate adsorption mode (see Table 1 for the Ag–O bonds) because the interaction of a silver NP with a negatively charged oxygen ($R–O^{-}$) is stronger than with a protonated oxygen atom (R–OH). Furthermore, the protonation of the phosphonate function adds steric hindrance, which also modifies the adsorption geometry of the molecule on the silver surface and the Raman patterns between 700 and 1200 cm^{-1} as discussed above.

In addition to the determination of the adsorption mode, we also compared the adsorption energies of the different protonated forms of the methylphosphonic acid onto the silver cluster (Table 1). The doubly deprotonated acid has the largest binding energy due to the strong tripod interaction of the three oxygen atoms with three silver atoms of the surface. The protonation of the phosphonate function leads to a significant decrease in the adsorption energy (Table 1). To be SERS active, the binding energy of the methylphosphonic acid should be larger than the one of the stabilizing agent (H_3BO_3). Since the stabilizing agent is in excess in solution, a trimeric structure able to block one adsorption site composed of three silver atoms can be formed. Therefore, three H_3BO_3 molecules must be displaced to accommodate the adsorption of one methylphosphonic molecule. The doubly deprotonated form, singly deprotonated form and totally protonated form respectively have an adsorption energy much higher (+29.6 kcal mol^{-1}), similar (within the numerical accuracy) and much lower (−8.3 kcal mol^{-1}) than the adsorption energy of the trimeric stabilizing agent. Therefore, only the doubly and

singly deprotonated form should be active in SERS, as observed experimentally.

(b) The effect of methylation

The adsorption energies were calculated to assess the steric effect induced by the methylation of the methylphosphonic acid into methyl hydrogen methylphosphonate and dimethyl methylphosphonate. The methylation of the phosphonate (Fig. 3) affects the adsorption modes in a way similar to that observed for protonation. However, the steric effects are larger since the hydrogen atom is replaced by a methyl group. As a consequence, the interaction of the methylated oxygen with the cluster is destabilized, which results in a longer Ag–OCH_3 bond compared with Ag–OH and lower binding energies (Table 1). No experimental spectrum has been recorded because the methylated molecules were not SERS active, which is in agreement with the computed adsorption energies that are lower (for CH_3–$PO(OCH_3)_2$) or equal within numerical accuracy (for CH_3–$PO_2(OCH_3)^-$) to the adsorption energy of the stabilizing agent (Table 1).

(c) The effect of the side chain.

The relative affinity of the phosphonate function associated with competitive amino and carboxylate functions of the side chain was studied by investigating the adsorption of the aminomethylphosphonic acid (AMPA) and the *N*-phosphonomethyl glycine (glyphosate). The computation of the electronic structure of AMPA and glyphosate has been performed for different protonation forms of each acidic function. The adsorption energies are reported in Table 1.

We first discuss the adsorption of the AMPA molecule. As for the methylphosphonic acid, SERS spectra were measured at two values of pH, at pH = 7.5 and pH = 10.5. However, the molecule can be protonated not only at the phosphonate function but also on the amine, which results in three pK_a (pK_{a_1} = 1.8, pK_{a_2} = 5.4, pK_{a_3} = 10) and four protonated forms that are labeled θ_0 to θ_3 where θ_x is the protonation form of the target molecule in which x acidic protons are lost by the molecule. At pH = 7.5 and pH = 10.5, the θ_2 and θ_3 forms respectively dominate in solution. The SERS spectra of AMPA at pH = 7.5 and pH = 10.5 exhibit the same number of peaks at similar Raman shifts as the methylphosphonic acid's spectra at pH = 4 and pH = 9, which indicates that the adsorption occurs through the phosphonate function. The spectrum of the θ_2 form has a double band around 800 cm^{-1} while the spectrum of the θ_3 form only has one, indicating that one of the oxygen atoms is protonated in the θ_2 form.

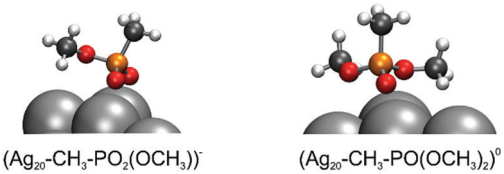

Fig. 3 Equilibrium geometries of the methyl hydrogen methylphosphonate CH_3–$PO_2(OCH_3)^-$ and dimethyl methylphosphonate CH_3–$PO(OCH_3)_2$ on silver cluster.

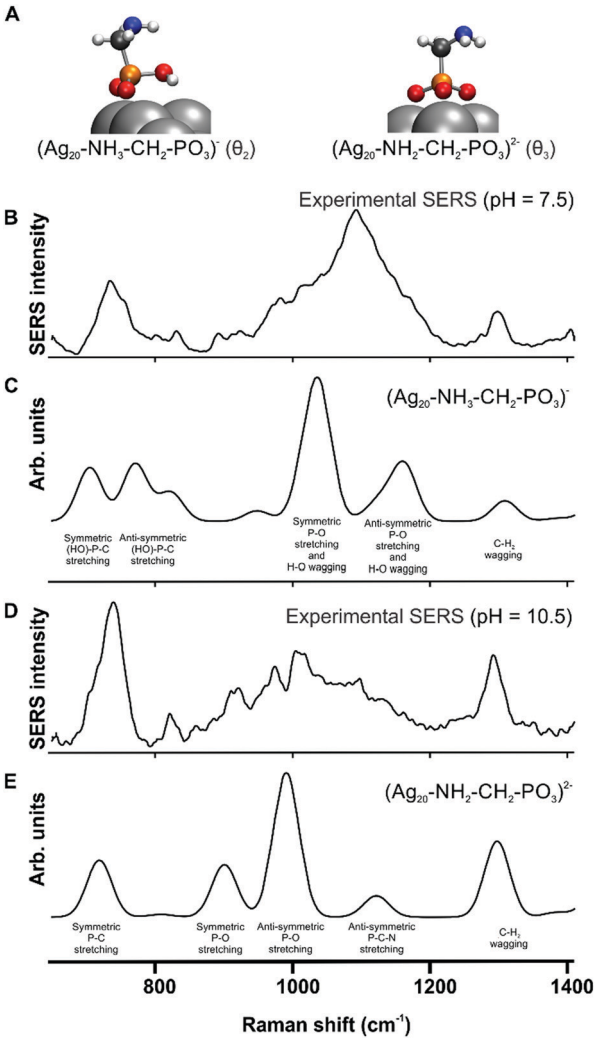

Fig. 4 (A) Equilibrium geometries of the $(Ag_{20}–AMPA(\theta_3))^{2-}$ and $(Ag_{20}–AMPA(\theta_2))^-$ complexes. (B) Measured SERS spectrum of AMPA measured at pH = 7.5, where there is 80% of the monoanionic form of AMPA θ_2. (C) Computed Raman spectrum of the lowest energy isomer of the $(Ag_{20}–AMPA(\theta_2))^-$ complex shown in panel A. (D) The experimental SERS spectrum of AMPA measured at pH = 10.5 where the AMPA θ_3 form dominates. (E) Thecomputed Raman spectrum of the lowest energy isomer of the $(Ag_{20}–AMPA\ (\theta_3))^-$ complex shown in panel A.

The AMPA molecule can be adsorbed perpendicularly to the cluster surface by the phosphonate or by the amine functional group, or it can also be adsorbed by both the amine and phosphonate groups lying parallel to the surface (see ESI†). Electronic structure computations show that the tripod adsorption by the phosphonate is the most stable isomer (Fig. 4A). The Raman spectrum of Ag_{20}–AMPA(θ_2) and Ag_{20}–AMPA(θ_3) where the adsorption occurs through the phosphonate function are overall in good agreement with the experimental one (Fig. 4). The main difference between the two charged species lies in the lowest band that is composed of a double peak for Ag_{20}–AMPA(θ_2) and a single peak for Ag_{20}AMPA(θ_3) as observed in the SERS spectra of $MePO_3H^-$ and $MePO_3^{2-}$, respectively, see

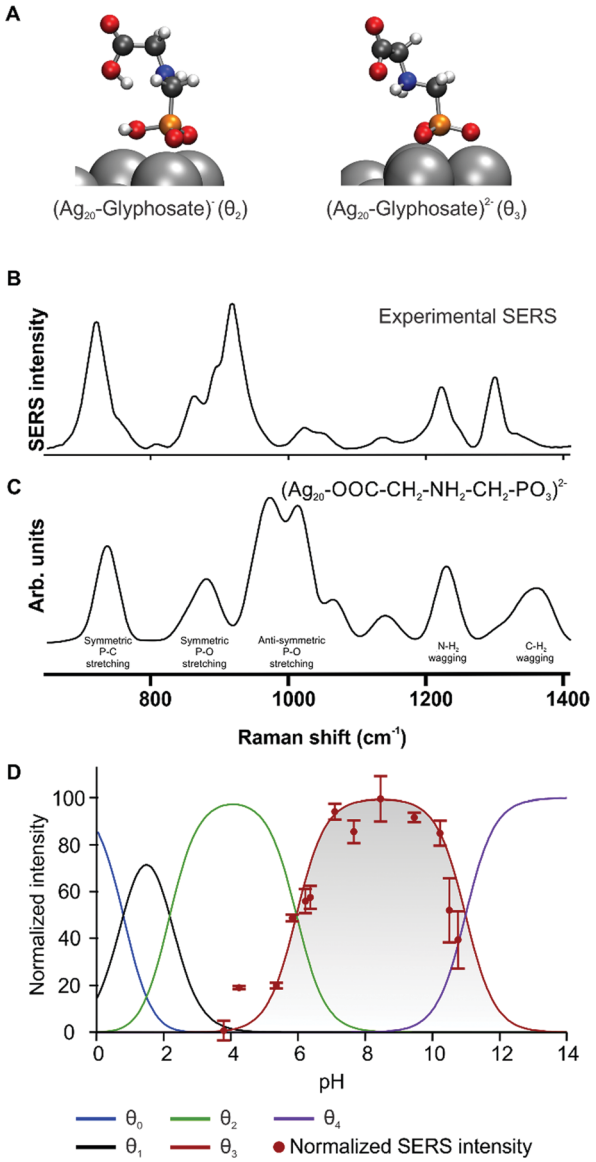

Fig. 5 (A) Equilibrium geometries of the isomers of the Ag_{20}–glyphosate (θ_2 and θ_3) complexes. (B) Experimental SERS spectrum of glyphosate measured at pH = 8. (C), and computed Raman spectra of the complex $(Ag_{20}–glyphosate)^{2-}$ (θ_3). (D) Fractional composition curves of the 5 forms of glyphosate in aqueous solution as a function of pH. The red dots represent the intensity of the SERS signal.

Fig. 2 above. In the case of AMPA too, the computed P–C band is red shifted because explicit solvation effects are not taken into account and the broad Raman pattern between 900 and 1200 cm^{-1} in the experimental spectrum reflects the multiple sites of similar binding energies that are possible at the surface of the NP.

We now turn to the adsorption of the glyphosate, a molecule characterized by a longer side chain than AMPA. Unlike AMPA, glyphosate has a carboxylate function at one of its extremities, which does not significantly alter the adsorption mode but strongly lowers the binding energies (Table 1). The molecule has 4 acidic protons (pK_{a_1} = 0.78, pK_{a_2} = 2.29, pK_{a_3} = 5.96, pK_{a_4} = 10.98)[26] that could play a role in the interaction with the silver surface. SERS spectra of glyphosate have therefore been recorded at different pH values ranging from 4 to 10, where silver nanoparticles are stable in solution. Within that pH range, the intensity of the SERS signal perfectly matches the fractional composition curve of the θ_3 form of the glyphosate (Fig. 5D), which is correlated to the concentration of the θ_3 form of the glyphosate in solution. It is therefore possible to consider a quantification of glyphosate at pH = 8 where the majority of the molecules are in the θ_3 form in solution.

The computed binding energies of the lowest energy isomers of θ_3 $(OOC–CH_2–NH_2–CH_2–PO_3)^{2-}$ and θ_2 $(OOC–CH_2–NH_2–CH_2–PO_3H)^-$ complexes show that only the θ_3 complex should be SERS active, in agreement with the experimental measurements. For the lowest energy isomer, the adsorption occurs through the phosphonate function in a tripod configuration as for the other studied molecules. All the other adsorption modes (through the amine or carboxylate) have significantly lower binding energies and are not likely present in solution. The computed Raman spectrum is in good agreement with the SERS spectrum, supporting that the adsorption occurs through the phosphonate function. The assignment of the vibrational modes is provided in Fig. 5.

The SERS spectra of AMPA and glyphosate are relatively similar but differ by Raman bands specific to the side chain. For example, a Raman band at 1293 cm^{-1} (NH_2 wagging) is observed in the SERS spectrum of both molecules, while a new Raman band appears at 1379 cm^{-1} (CH_2 wagging) only for the glyphosate. Therefore, this family of molecules which possess similar chemical structure and exhibit identical types of interactions with the silver cluster be could be differentiated by their SERS spectrum and quantified under specific pH conditions.

Conclusion

Optimized SERS developments for analytical purposes are often simply established by a trial and error approach due to the large number of dependent experimental parameters that can affect the SERS signals. Although this can be effective in some simple cases, it can rapidly turn into a laborious process. An improved understanding of the surface chemistry is needed, particularly if the nanoparticle substrate is in contact with aqueous media. We have seen the role played by the protonation and the methylation of the phosphonate function but also the effect of the substitution of its side chains. Combining a computational approach with experimental data provided here the necessary tools for a better understanding of the physico-chemical phenomena at the nanoparticle surface leading to SERS activity, SERS affinity and the adsorption mechanism of the studied molecules on a silver nanoparticle. This work presents breakthrough concepts and protocols for simultaneous detection of phosphonated molecules creating real opportunities in key areas such as environmental and water resource *in situ* monitoring by a portable Raman spectrometer.

Conflicts of interest

There are no conflicts to declare.

Acknowledgements

The authors acknowledge the support of the RU MolSys at the University of Liège. F. R. and B. M. acknowledge support from the Fonds National de la Recherche Scientifique, Belgium. Computational resources have been provided by the Consortium des Equipements de Calcul Intensif (CéCI), funded by the Fonds de la Recherche Scientifique of Belgium (F.R.S.-FNRS) under Grant No. 2.5020.11.

Notes and references

1 J. Galezowska and E. Gumienna-Kontecka, *Coord. Chem. Rev.*, 2012, **256**, 105–124.
2 M. Liong, J. Lu, M. Kovochich, T. Xia, S. G. Ruehm, A. E. Nel, F. Tamanoi and J. I. Zink, *ACS Nano*, 2008, **2**, 889–896.
3 R. Li, Z. Ji, J. Dong, C. H. Chang, X. Wang, B. Sun, M. Wang, Y. P. Liao, J. I. Zink, A. E. Nel and T. Xia, *ACS Nano*, 2015, **9**, 3293–3306.
4 S. G. Penn, L. He and M. J. Natan, *Curr. Opin. Chem. Biol.*, 2003, **7**, 609–615.
5 J. C. S. Costa, R. a. Ando, A. C. Sant'Ana and P. Corio, *Phys. Chem. Chem. Phys.*, 2012, **14**, 15645.
6 S. Pang, T. Yang and L. He, *TrAC, Trends Anal. Chem.*, 2016, **85**, 73–82.
7 J. Wang and P. Somasundaran, *J. Colloid Interface Sci.*, 2005, **291**, 75–83.
8 P. Maksymovych, D. C. Sorescu and J. T. Yates, *J. Phys. Chem. B*, 2006, **110**, 21161–21167.
9 G. D. Fleming, J. Villagrán and R. Koch, *Spectrochim. Acta, Part A*, 2013, **114**, 120–128.
10 M. Pagliai, S. Caporali, M. Muniz-Miranda, G. Pratesi and V. Schettino, *J. Phys. Chem. Lett.*, 2012, **3**, 242–245.
11 J. R. Lombardi and R. L. Birke, *Acc. Chem. Res.*, 2009, **42**, 734–742.
12 K. Kneipp, H. Kneipp and H. G. Bohr, *Top. Appl. Phys.*, 2006, **103**, 261–278.
13 E. Podstawka, T. K. Olszewski, B. Boduszek and L. M. Proniewicz, *J. Phys. Chem*, 2009, **113**, 12013–12018.
14 E. Proniewicz, N. Piergies, Y. Ozaki, Y. Kim and L. M. Proniewicz, *Spectrochim. Acta, Part A*, 2013, **103**, 167–172.
15 N. Piergies, E. Proniewicz, Y. Kim and L. M. Proniewicz, *J. Raman Spectrosc.*, 2014, **45**, 581–590.
16 J. A. Creighton, C. G. Blatchford and M. G. Albrecht, *J. Chem. Soc., Faraday Trans. 2*, 1979, **75**, 790–798.
17 H. Krawczyk, *Synth. Commun.*, 1997, **27**, 3151–3161.
18 K. Kneipp, M. Moskovits and H. Kneipp, *Surface-Enhanced Raman Scattering: Physics and applications*, Springer, Berlin, 2006.
19 S. Lin and M. R. Wiesner, *Langmuir*, 2012, **28**, 11032–11041.
20 M. Frisch, G. W. Trucks, H. B. Schlegel, G. E. Scuseria, M. A. Robb, J. R. Cheeseman, G. Scalmani, V. Barone, B. Mennucci and G. A. Petersson, *Gaussian 09, Revision E.01*, Inc., Wallingford, CT, 2009.
21 J.-D. Chai and M. Head-Gordon, *Phys. Chem. Chem. Phys.*, 2008, **10**, 6615.
22 P. J. Hay, W. R. Wadt, P. J. Hay and W. R. Wadt, *J. Chem. Phys.*, 1985, **82**, 270–283.
23 J. E. Moore, S. M. Morton and L. Jensen, *J. Phys. Chem. Lett.*, 2012, **3**, 2470–2475.
24 P. Borowski, W. Gac, P. Pulay and K. Wolin, *New J. Chem.*, 2016, **40**, 7663–7670.
25 E. Koglin and J.-M. Séquaris, *Top. Curr. Chem.*, 1986, **134**, 1–57.
26 K. Chamberlain, A. A. Evans and R. H. Bromilow, *Pestic. Sci.*, 1996, **47**, 265–271.

